Rotatory power reversal induced by magnetic current in bi-isotropic media

Pedro D. S. Silva* and Manoel M. Ferreira, Jr.†
Departamento de Física, Universidade Federal do Maranhão, Campus Universitário do Bacanga, São Luís (MA), 65080-805, Brazil

(Received 11 July 2022; accepted 6 October 2022; published 25 October 2022)

Bi-isotropic media constitute a proper scenario for scrutinizing optical effects stemming from magnetoelectric parameters. Chiral magnetic current is a macroscopic effect arising from the chiral magnetic effect that enriches the phenomenology of a classical dielectric medium. This paper examines the optical aspects of bi-isotropic media in the presence of Ohmic and magnetic conductivity. The full isotropic scenario manifests circular birefringence described by a dispersive rotatory power that changes sign at a given frequency. For a bi-isotropic medium with antisymmetric magnetic conductivity, an intricate dispersive rotatory power is attained, supplied with sign reversal as well. This scenario occurs in the absence or presence of Ohmic conductivity. It also indicates a handedness reversion of the medium, an unusual property in dielectrics, which may work as a signature of bi-isotropic media supporting chiral magnetic current.

DOI: 10.1103/PhysRevB.106.144430

I. INTRODUCTION

The classical propagation of electromagnetic waves in continuous matter is ruled by the Maxwell equations and the constitutive relations that enclose the response to applied electromagnetic fields [1,2]. In linear electrodynamics, a great diversity of electromagnetic phenomena in continuous media can be accounted for by general constitutive relations,

$$D^i = \epsilon_{ij}E^j + \alpha_{ij}B^j, \tag{1a}$$

$$H^i = \mu_{ij}^{-1}B^j + \beta_{ij}E^j, \tag{1b}$$

where ϵ_{ij} and μ_{ij} are the electric permittivity and magnetic permeability tensors, while α_{ij} and β_{ij} are magnetoelectric parameters that capture the electric (magnetic) response to applied magnetic (electric) field, respectively. In the simplest scenario, relations (1) read

$$\begin{pmatrix}\mathbf{D}\\ \mathbf{H}\end{pmatrix} = \begin{pmatrix}\epsilon & \alpha\\ \beta & \mu^{-1}\end{pmatrix}\begin{pmatrix}\mathbf{E}\\ \mathbf{B}\end{pmatrix}, \tag{2}$$

where ϵ, α, β, μ are parameters composing the bi-isotropic linear connection between ($\mathbf{D}$, $\mathbf{H}$) and ($\mathbf{E}$, $\mathbf{B}$) for homogenous nondispersive materials [3,4].

In the last decades, bi-isotropic relations have been extensively investigated [5–9], being also important to address the properties of topological insulators [10–16] and axion electrodynamics [17–19]. In nonlinear electrodynamics, the constitutive tensors usually depend on the electric and magnetic fields, providing a way to describe well-known phenomena, e.g., the Kerr and Cotton-Mouton effects [20]. Most recently, nonlinear electrodynamics addressing axion-photon couplings has been reported [21], where general nonlinear permittivity and permeability tensors present a dependence on the frequency, wave vector, and axion mass. Other aspects of nonlinearities in constitutive tensors, such as the description of ferrimagnetic materials and radiation produced by a charged particle interacting with a nonlinear medium, have also been examined [22], in the context of nonlinear electrodynamics [23].

For scenarios where the constitutive parameters in Eq. (1) are complex tensors, they characterize bianisotropic media [24,25], also known as chiral materials [26–29]. A medium is named chiral when it lacks inversion symmetry, that is, when it is parity-odd, or, in other words, when it is invariant only under the L_0 component of the Lorentz group [30]. A chiral scenario, realized by constitutive relations (2) with complex parameters, was used to examine the Fresnel equations that describe reflection, refraction, and the Brewster angle [30]. Right-handed (RCP) and left-handed circularly polarized (LCP) waves are examples of electromagnetic chiral phenomena, which in an achiral medium propagate at the same phase velocity, yielding no anisotropy effect. In a chiral medium, however, the LCP and RCP waves travel at distinct phase velocities (related to different refractive indices), implying the birefringence (which causes optical rotation)[1] [31–35]. It is known that the optical rotation stems from the natural optical activity of the medium or can be induced by external fields, as it occurs in the Faraday effect [36–38]. Magneto-optical effects constitute a useful probe to investigate topological insulators [39–41] and new materials [42,43].

When the optical rotation depends on the frequency, there occurs rotatory power (RP) dispersion. If it depends on

*pedro.dss@discente.ufma.br; pdiego.10@hotmail.com
†manojr.ufma@gmail.com

[1]It refers to the rotation of the plane of vibration of the electric field which occurs while the linearly polarized wave propagates through the chiral medium. This is a consequence of birefringence, a phenomenon quantified or measured in terms of the rotation angle per unit length (rotatory power).

the frequency and undergoes reversion, it is called anomalous RP dispersion [44,45]. Thus, the RP analysis is a relevant tool to describe the optical properties of several systems, such as crystals [46,47], organic compounds [32,48], rotating plasma and neutron stars [49,50], graphene terahertz magneto-optical phenomena [51], gas of fast-spinning molecules [52,53], entangled photons in quantum optics [54], and chiral metamaterials [55,56]. In addition to birefringence, circular dichroism, the difference in the absorption of LCP and RCP light, is also used to probe the optical activity of materials. Dichroism can work as a tool to distinguish between Dirac and Weyl semimetals [57], perform enantiomeric discrimination [58,59], and for developing graphene-based devices at terahertz frequencies [60].

Another phenomenon that has caught attention in the context of continuous media is the chiral magnetic effect (CME), which involves a macroscopic generation of an electric current in the presence of a magnetic field as the result of an asymmetry between the number density of left- and right-handed chiral fermions [61–65]. In condensed-matter systems, the CME plays a relevant role in Weyl semimetals, where it is usually connected to the chiral anomaly associated with Weyl nodal points [66], but also takes place in the absence of Weyl nodes [67]. We mention other investigations on this subject, for instance, the anisotropic effects stemming from tilted Weyl cones [68], the CME and anomalous transport in Weyl semimetals [69], quantum oscillations arising from the CME [70], the determination of electromagnetic fields produced by an electric charge near a topological Weyl semimetal with two Weyl nodes [71], solutions of axion electrodynamics [72], and renormalization evaluations for Weyl semimetals and Dirac materials [73].

Weyl semimetals also present CME, whose classical description stems from an axion term Lagrangian [17,72,74–76]

$$\mathcal{L} = \theta(\mathbf{E}\cdot\mathbf{B}), \tag{3}$$

which implies corrections to the Maxwell nonhomogeneous equations,

$$\begin{aligned} \boldsymbol{\nabla}\cdot\mathbf{E} &= \rho - \boldsymbol{\nabla}\theta\cdot\mathbf{B}, \\ \boldsymbol{\nabla}\times\mathbf{B} - \partial_t\mathbf{E} &= \mathbf{j} + (\partial_t\theta)\mathbf{B} + \boldsymbol{\nabla}\theta\times\mathbf{E}, \end{aligned} \tag{4}$$

where $\boldsymbol{\nabla}\theta\cdot\mathbf{B}$ is an anomalous charge density, $\boldsymbol{\nabla}\theta\times\mathbf{B}$ is a kind of anomalous Hall effect, and $(\partial_t\theta)\mathbf{B}$ plays the role of the chiral magnetic current. Such terms were also examined in Ref. [76], where stationary classical solutions for chiral matter were also carried out.

In the case the axion coupling does not depend on space coordinates, $\boldsymbol{\nabla}\theta = \mathbf{0}$, the Maxwell equations (4) simplify as

$$\boldsymbol{\nabla}\cdot\mathbf{E} = \rho, \quad \boldsymbol{\nabla}\times\mathbf{B} - \partial_t\mathbf{E} = \mathbf{j} + (\partial_t\theta)\mathbf{B}, \tag{5}$$

providing an electrodynamics with chiral magnetic current, $(\partial_t\theta)\mathbf{B}$, but deprived of the anomalous charge and anomalous Hall terms. This is the case to be considered in the present paper.

In an effective approach, the magnetic current can be introduced using a general constitutive relation for the current density

$$J^i = \sigma E^i + \sigma^B_{ij}B^j, \tag{6}$$

where σ is the Ohmic conductivity and σ^B_{ij} is the chiral magnetic-conductivity general tensor. A dielectric medium supporting such a magnetic current has been recently examined for symmetric and antisymmetric conductivity tensors [77], with the determination of the refractive indices, propagating modes, and some optical properties. The antisymmetric scenario for σ^B was realized in some Weyl semimetals [78]. The interplay between Lorentz-violating electrodynamics, optical effects, and condensed-matter physics [79,80] has also been explored.

Considering the relevance of optical effects for describing material properties, in this paper we investigate the propagation of electromagnetic waves in bi-isotropic media endowed with magnetic conductivity, a type of chiral scenario. We first address a bi-isotropic dielectric with an isotropic current constitutive relation, focusing on the birefringence and rotatory power. We obtain a linearly dispersive RP with sign reversion. Afterwards, we develop the same analysis for an antisymmetric conductivity tensor, attaining an involved dispersive RP which also exhibits a sign change. These results may also cause handedness reversal of the medium. This paper is outlined as follows: In Sec. II we present the general framework to obtain the dispersion relations, refractive indices, and propagating modes. In Sec. III, we address a bi-isotropic medium in the presence of isotropic and antisymmetric magnetic conductivity and examine the results. Finally, we summarize our results in Sec. IV.

II. DISPERSION RELATION FOR BI-ISOTROPIC MEDIUM ENDOWED WITH OHMIC AND CHIRAL CURRENT

We take as a starting point the Maxwell equations for a homogeneous and linear chiral medium, here written in accordance with a plane-wave ansatz,

$$\mathbf{k}\cdot\mathbf{D} = \rho, \quad \mathbf{k}\times\mathbf{H} + \omega\mathbf{D} = -i\mathbf{J}, \tag{7a}$$

$$\mathbf{k}\cdot\mathbf{B} = 0, \quad \omega\mathbf{B} = \mathbf{k}\times\mathbf{E}, \tag{7b}$$

where ρ is the charge density and the constitutive relation for the current density is given in Eq. (6). Here, we suppose the magnetic current is the only chiral contribution in this medium, being associated with the axion term $(\partial_t\theta)\mathbf{B}$ of Eq. (5). In some Weyl semimetal, the carrier density is very low [72] so that one can consider $\rho = 0$ and $\sigma = 0$, and the current density reads

$$J^i = \sigma^B_{ij}B^j. \tag{8}$$

However, when the carrier density is relatively large, one needs to consider $\rho \neq 0$ and the Ohmic current $\sigma \neq 0$ (see Sec. II B of Ref. [72]). In this case, the current density is the one of Eq. (6).

We now suppose the validity of isotropic-anisotropic constitutive relations, in which the anisotropy is constrained into the magnetoelectric parameters, that is, the electric permittivity and magnetic permeability are written as

$$\mu^{-1}_{ka} = \mu^{-1}\delta_{ka}, \quad \epsilon_{ij} = \epsilon\delta_{ij}, \tag{9}$$

so that the constitutive relations (1) take the form

$$D^i = \epsilon\delta_{ij}E^j + \alpha_{ij}B^j, \tag{10a}$$

$$H^i = \beta_{ij}E^j + \mu^{-1}\delta_{ij}B^j. \tag{10b}$$

For obtaining wave equations that describe the propagation of electromagnetic waves in such a dielectric medium, we replace the constitutive relation (10a) in the second relation of Eq. (7a) with the current density of Eq. (6). We also employ the Faraday's law, $\omega\mathbf{B} = \mathbf{k}\times\mathbf{E}$, writing

$$\frac{1}{\mu\omega}[\mathbf{k}\times(\mathbf{k}\times\mathbf{E})]^i + \omega\epsilon\delta_{ij}E^j + \beta_{ka}\epsilon_{ijk}k^jE^a + \alpha_{ij}\epsilon_{jmn}k^mE^n = -i\sigma E^i - i\sigma^B_{ij}B^j. \tag{11}$$

Using again the Faraday's law, Eq. (11) is rewritten as

$$[\mathbf{k}\times(\mathbf{k}\times\mathbf{E})]^i + \omega^2\mu\bar{\epsilon}_{ij}E^j = 0, \tag{12}$$

where the frequency-dependent extended permittivity tensor,

$$\bar{\epsilon}_{in}(\omega) = \tilde{\epsilon}\delta_{in} + \frac{1}{\omega}\left(\beta_{kn}\epsilon_{imk} + \alpha_{ij}\epsilon_{jmn} + i\frac{\sigma^B_{ij}}{\omega}\epsilon_{jmn}\right)k^m, \tag{13}$$

carries the electric and magnetic response of the medium and also comprises the permittivity of a usual conductor,

$$\tilde{\epsilon} = \epsilon + i\frac{\sigma}{\omega}. \tag{14}$$

Equation (12) can be cast in the form

$$M_{ij}E^j = 0, \tag{15}$$

where the tensor M_{ij} is given in terms of the refractive index $\mathbf{n}$ as

$$M_{ij} = n^2\delta_{ij} - n_in_j - c^2\mu\bar{\epsilon}_{ij}. \tag{16}$$

We have used $\mathbf{k} = \omega\mathbf{n}/c$, with c being the vacuum light speed. Here, we consider that the index $\mathrm{Re}[n]$ is non-negative, so that we adopt $n = +\sqrt{\mathbf{n}^2}$, instead of $|\mathbf{n}|$, in order to permit complex refractive indices. The refractive indices with negative real parts, related to metamaterials, are not considered here. To find the nontrivial solution for the electric field of Eq. (15), we impose the condition $\det[M_{ij}] = 0$ in order to attain the dispersion relations that govern the wave propagation in the medium.

III. DISPERSION RELATIONS, REFRACTIVE INDICES, AND PROPAGATING MODES

In this section, we examine the propagation of electromagnetic waves in a dielectric medium under the validity of the relations (12) and (13) for two configurations of magnetic conductivity: the symmetric isotropic one and the antisymmetric one.

A. Full isotropic case

In the context of the constitutive relations (10), we begin by considering the total symmetric isotropic configuration for the quantities α_{ij}, β_{ij}, and σ^B_{ij}, in which these tensors are written as diagonal tensors, namely

$$\alpha_{ij} = \alpha\delta_{ij}, \quad \beta_{ij} = \beta\delta_{ij}, \quad \sigma^B_{ij} = \Sigma\delta_{ij}, \tag{17}$$

with $\alpha,\ \beta \in \mathbb{C}$, and $\Sigma \in \mathbb{R}$. The condition $\alpha_{ij} = -\beta^\dagger_{ij}$ for electromagnetic energy conservation [28], when applied on the parametrization of Eq. (17), yields

$$\beta^* = -\alpha. \tag{18}$$

In this case, the constitutive relations take on the typical bi-isotropic form,

$$\mathbf{D} = \epsilon\mathbf{E} + \alpha\mathbf{B}, \tag{19a}$$

$$\mathbf{H} = \frac{1}{\mu}\mathbf{B} + \beta\mathbf{E}, \tag{19b}$$

$$\mathbf{J} = \sigma\mathbf{E} + \Sigma\mathbf{B}, \tag{19c}$$

the last one being the isotropic magnetic current. As already mentioned, such relations play a relevant role in topological insulators [10–16] and axion systems [17–19].

Inserting relations (17) in Eq. (13), one obtains

$$c\bar{\epsilon}_{ij} = c\tilde{\epsilon}\delta_{ij} - \left(\alpha + \beta + i\frac{\Sigma}{\omega}\right)\epsilon_{ijm}n^m, \tag{20}$$

where the last term on the right-hand side represents the "magnetic-electric" contribution to the medium permittivity. In this case, the tensor M_{ij} (16) has the form

$$[M_{ij}] = \mathcal{M} + \mu c\left(\alpha + \beta + i\frac{\Sigma}{\omega}\right)\mathcal{S}, \tag{21a}$$

where

$$\mathcal{M} = (n^2 - c^2\mu\tilde{\epsilon})\mathbb{1}_3 - \begin{pmatrix} n_1^2 & n_1n_2 & n_1n_3 \\ n_1n_2 & n_2^2 & n_2n_3 \\ n_1n_3 & n_2n_3 & n_3^2 \end{pmatrix}, \tag{21b}$$

and

$$\mathcal{S} = \begin{pmatrix} 0 & -n_3 & n_2 \\ n_3 & 0 & -n_1 \\ -n_2 & n_1 & 0 \end{pmatrix}. \tag{21c}$$

Requiring $\det[M_{ij}] = 0$, one gets

$$n^4 - n^2c^2\left[2\mu\tilde{\epsilon} - \mu^2\left(\alpha + \beta + i\frac{\Sigma}{\omega}\right)^2\right] + \mu^2\tilde{\epsilon}^2c^4 = 0. \tag{22}$$

Solving for n, we obtain the following refractive indices,

$$n_\pm = c\sqrt{\mu\tilde{\epsilon} - Z} \pm ic\sqrt{Z}, \tag{23}$$

with

$$Z = \frac{\mu^2}{4}\left(\alpha + \beta + i\frac{\Sigma}{\omega}\right)^2. \tag{24}$$

As we have started with isotropic tensors, $\epsilon\delta_{ij}$, $\mu^{-1}\delta_{ij}$, $\alpha\delta_{ij}$, $\beta\delta_{ij}$, any arising anisotropy effects stem from the way magnetoelectric and magnetic conductivity are coupled to the fields in the constitutive relations (19).

1. Propagation modes

In order to achieve the propagating modes, we write the refractive indices (23) as

$$n_\pm^2 = c^2\mu\tilde{\epsilon} \pm 2ic\sqrt{Z}n_\pm, \tag{25}$$

and replace them in the matrix (21), so that Eq. (15) yields

$$\mathbf{E}_{\pm} = \frac{1}{\sqrt{2}n\sqrt{n^2 - n_1^2}} \begin{pmatrix} n^2 - n_1^2 \\ \pm inn_3 - n_1 n_2 \\ \mp inn_2 - n_1 n_3 \end{pmatrix}. \tag{26}$$

Now, we consider the specific case of propagation along the z axis, $\mathbf{n} = (0, 0, n)$, in such a way that Eq. (26) provides right-handed ($\hat{\mathbf{E}}_-$) and left-handed circular ($\hat{\mathbf{E}}_+$) polarization vectors, respectively [1,2],

$$\mathbf{E}_{\pm} = \frac{1}{\sqrt{2}} \begin{pmatrix} 1 \\ \pm i \\ 0 \end{pmatrix}. \tag{27}$$

As well known, the circular polarization modes (27) open the possibility for the attainment of circular birefringence in this system.

2. *Optical effects of complex magnetoelectric parameters in nonconducting dielectrics*

As the modes (27) do not depend on the real or complex character of the parameters α and β, we will examine both situations. In this sense, we suppose α and β as complex parameters,

$$\alpha = \alpha' + i\alpha'', \quad \beta = \beta' + i\beta'', \tag{28}$$

where $\alpha' = \mathrm{Re}[\alpha]$, $\alpha'' = \mathrm{Im}[\alpha]$, $\beta' = \mathrm{Re}[\beta]$, and $\beta'' = \mathrm{Im}[\beta]$. The condition (18) then implies

$$\alpha' = -\beta', \quad \alpha'' = \beta'', \tag{29}$$

so that

$$\alpha + \beta = 2i\alpha''. \tag{30}$$

In order to examine the physical behavior stemming from the constitutive relations (19a)–(19c), we rewrite the refractive index (23) using Eq. (30), that is,

$$n_{\pm} = c\sqrt{\mu\tilde{\epsilon} + \mu^2\left(\alpha'' + \frac{\Sigma}{2\omega}\right)^2} \mp \mu c\left(\alpha'' + \frac{\Sigma}{2\omega}\right). \tag{31}$$

Remembering the complex piece of $\tilde{\epsilon}$ inside the root, the refractive index can be rewritten as

$$n_{\pm} = \Upsilon_+ \mp \mu c\left(\alpha'' + \frac{\Sigma}{2\omega}\right) + i\Upsilon_-, \tag{32}$$

where

$$\Upsilon_{\pm} = c\sqrt{\frac{R}{2}}\sqrt{\sqrt{1 + \left(\frac{\mu\sigma}{\omega R}\right)^2} \pm 1}, \tag{33}$$

$$R = \mu\epsilon + \mu^2\left(\alpha'' + \frac{\Sigma}{2\omega}\right)^2. \tag{34}$$

Equation (32) represents refractive indices with positive and distinct real pieces, implying birefringence. Both isotropic Ohmic and magnetic-conductivity Σ appear as frequency-dependent contributions, which bring about a dispersive behavior to the system. Since the propagating modes are described by circularly polarized vectors [see Eq. (27)], the rotatory power can be evaluated in terms of the difference between the refractive indices [33,36,79],

$$\delta = -\frac{[\mathrm{Re}(n_+) - \mathrm{Re}(n_-)]\omega}{2c}, \tag{35}$$

as a consequence of birefringence. With indices (31), it yields

$$\delta = \frac{\mu\Sigma}{2} + \mu\omega\alpha''. \tag{36}$$

It displays a zeroth-order term in the frequency that recovers the same rotatory power of isotropic case of Ref. [77] when $\alpha'' = 0$. For a negative α'', the rotatory power reads

$$\delta = \frac{\mu\Sigma}{2} - \mu\omega|\alpha''|. \tag{37}$$

From Eq. (37), one finds a cutoff frequency ω',

$$\omega' = \frac{\Sigma}{2|\alpha''|}, \tag{38}$$

defining the value at which the sign reversion of δ occurs. Considering the usual RP sign convention [33] and Eq. (37), one notices the following: (1) For $0 < \omega < \omega'$, one has $\delta > 0$, causing a clockwise rotation of the linear electric field polarization. (2) For $\omega > \omega'$, one finds $\delta < 0$, implying a counterclockwise rotation of the linear polarization.

As this RP inversion takes place at a positive frequency, $\omega' > 0$, one needs to have either $\Sigma < 0$ or $\alpha'' < 0$. In the following we shall consider $\alpha'' < 0$. The RP reversion observed here is not usual in ordinary linear dielectric nor in bi-isotropic or bianisotropic dielectric media. It also does not appear in media endowed with isotropic magnetic conductivity [77] [see Eq. (39)]. However, it is reported in rotating plasmas [49] and graphene systems [51]. Furthermore, as shown in Eq. (37), such an effect also appears in a bi-isotropic dielectric under the presence of the magnetic current (19c). The general behavior of the rotatory power (37) as a function of frequency is illustrated in Fig. 1 for some values of Σ, α'', and μ. Finally, for $\omega = \omega'$, the birefringence does not occur ($\delta = 0$).

As a special case, we can address the case the system possesses only chiral conductivity, $\Sigma \neq 0$, $\sigma = 0$, for which

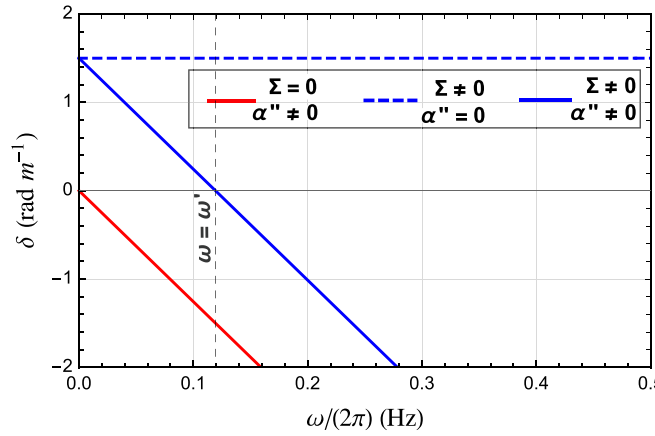

FIG. 1. Polarization rotation angle per length unit, as given in Eq. (37). Here, we have used $\mu = 1\ \mathrm{H\,m^{-1}}$, $\Sigma = 3\ \Omega^{-1}\,\mathrm{s^{-1}}$, and $|\alpha''| = 2\ \mathrm{F\,s^{-1}}$. The vertical dashed line is given by $\omega'/(2\pi) = 3/4$ Hz, with ω' of Eq. (38).

the refractive index (31) is written replacing $\tilde{\epsilon} \to \epsilon$, yielding an entirely real expression. The rotatory power (37) remains unmodified as far as all the analysis about its reversion. In this context, we can also consider the situation $\alpha, \beta \in \mathbb{R}$, for which one has simply $\beta = -\alpha$ and $\beta + \alpha = 0$, since $\alpha'' = 0$. Hence, Eq. (31) (with $\tilde{\epsilon} \to \epsilon$) becomes

$$n_\pm = c\sqrt{\mu\epsilon + \frac{\mu^2\Sigma^2}{4\omega^2}} \mp \frac{\mu c\Sigma}{2\omega}, \tag{39}$$

which also leads to birefringence, in this case stemming entirely from the magnetic conductivity. The corresponding rotatory power, $\delta = \mu\Sigma/2$, obviously does not undergo reversion.

B. Bi-isotropic case with off-diagonal antisymmetric magnetic-conductivity tensor

Let us now consider a substrate described by the bi-isotropic constitutive parameters in the presence of a chiral current written in terms of an antisymmetric magnetic conductivity, that is,

$$\alpha_{ij} = \alpha\delta_{ij}, \quad \beta_{ij} = \beta\delta_{ij}, \quad \sigma^B_{ij} = \epsilon_{ijk}b_k, \tag{40}$$

for which the permittivity (13) is

$$c\bar{\epsilon}_{ij} = \left[c\tilde{\epsilon} - \frac{i}{\omega}(\mathbf{b}\cdot\mathbf{n})\right]\delta_{ij} + (\alpha+\beta)\epsilon_{ijk}n_k + \frac{i}{\omega}n_i b_j. \tag{41}$$

The matrix $[M_{ij}]$ of Eq. (15) reads

$$[M_{ij}] = \mathcal{M} + \frac{i\mu c}{\omega}(\mathbf{b}\cdot\mathbf{n})\mathbb{1}_3 - \frac{i\mu c}{\omega}\mathcal{B}, \tag{42}$$

with $\mathcal{M}$ given by Eq. (21b) and

$$\mathcal{B} = \begin{pmatrix} n_1b_1 & -i\omega\gamma n_3 + n_1b_2 & i\omega\gamma n_2 + n_1b_3 \\ i\omega\gamma n_3 + n_2b_1 & n_2b_2 & -i\omega\gamma n_1 + n_2b_3 \\ -i\omega\gamma + n_3b_1 & i\omega\gamma n_1 + n_3b_2 & n_3b_3 \end{pmatrix}, \tag{43a}$$

and $\gamma = \alpha + \beta$. Evaluating $\det[M_{ij}] = 0$, one attains the following dispersion equation:

$$n^4 - 2n^2\left[\mu\tilde{\epsilon}c^2 - \frac{\mu^2c^2}{2}(\alpha+\beta)^2 - \frac{i\mu c}{\omega}(\mathbf{b}\cdot\mathbf{n})\right] + \mu^2c^2\left[c\tilde{\epsilon} - \frac{i}{\omega}(\mathbf{b}\cdot\mathbf{n})\right]^2 = 0. \tag{44}$$

Implementing $\mathbf{b}\cdot\mathbf{n} = bn\cos\theta$ in Eq. (44), we have a fourth-order equation in n. Searching for the solutions for n that recover the refractive indices of an ordinary dielectric, $n_\pm \mapsto c\sqrt{\mu\epsilon}$, in the limit of vanishing magnetoelectric and conductivity parameters, that is, $\gamma \mapsto 0$ and $b \mapsto 0$. We thus find

$$n_\pm = c\sqrt{\mu\tilde{\epsilon} - \frac{\mu^2}{4}\left(\gamma \mp \frac{b\cos\theta}{\omega}\right)^2} \pm \frac{i\mu c}{2}\left(\gamma \mp \frac{b\cos\theta}{\omega}\right). \tag{45}$$

The other two solutions of Eq. (44) that provide $n_\pm \mapsto -c\sqrt{\mu\epsilon}$ in the limit of an ordinary dielectric will not be considered here. Considering the relations (29), the refractive indices are rewritten now as

$$n_\pm = c\sqrt{\mu\tilde{\epsilon} - \frac{\mu^2}{4}\left(2i\alpha'' \mp \frac{b\cos\theta}{\omega}\right)^2} \mp \mu c\alpha'' - \frac{i\mu c}{2\omega}b\cos\theta. \tag{46}$$

1. Propagation modes

Let us consider the coordinate system where propagation is along the z axis, $\mathbf{n} = (0, 0, n)$, then Eq. (42) simplifies as

$$[M_{ij}] = (n^2 - c^2\mu\tilde{\epsilon})\mathbb{1}_3 + c\begin{pmatrix} +\frac{i\mu nb}{\omega}\cos\theta & -2i\mu\alpha''n & 0 \\ 2i\mu\alpha''n & +\frac{i\mu nb}{\omega}\cos\theta & 0 \\ -i\mu b_1 n/\omega & -i\mu b_2 n/\omega & -n^2/c \end{pmatrix}. \tag{47}$$

Rewriting Eq. (46) as

$$n_\pm^2 = c^2\mu\tilde{\epsilon} \pm i\mu c\left(2i\alpha'' \mp \frac{b}{\omega}\cos\theta\right)n_\pm, \tag{48}$$

and replacing it in Eq. (47), the condition (15) provides the following electric fields for the propagating modes,

$$\mathbf{E}_\pm = E_0\begin{pmatrix} 1 \\ \pm i \\ -in_\pm(b_1 \pm ib_2)/(\omega\tilde{\epsilon}c) \end{pmatrix}, \tag{49}$$

with an appropriately chosen amplitude E_0. Such fields stand for "mixed modes," composed of a circular polarization transversal sector and an additional longitudinal component. For the special case where the **b** vector is parallel or antiparallel to the propagation direction **n**, we set $\mathbf{b} = (0, 0, b_3)$, with which Eq. (49) yields

$$\mathbf{E}_\pm = E_0\begin{pmatrix} 1 \\ \pm i \\ 0 \end{pmatrix}, \tag{50}$$

representing left- and right-handed circularly polarized vectors, respectively.

2. Optical effects for case $\sigma^B_{ij} \neq 0$ and $\sigma = 0$

At first, we examine the particular case in which the medium has non-null magnetic conductivity and null Ohmic conductivity. With $\tilde{\epsilon} \to \epsilon$ the refractive indices of Eq. (46) become

$$n_\pm = c\sqrt{\mu\epsilon - \frac{\mu^2}{4}\left(2i\alpha'' \mp \frac{b\cos\theta}{\omega}\right)^2} \mp \mu c\alpha'' - \frac{i\mu c}{2\omega}b\cos\theta, \tag{51}$$

which can be expressed by separating the real and complex pieces,

$$n_\pm = UA_+ \mp \mu c\alpha'' + i\left(\pm UA_- - \frac{\mu c}{2\omega}b\cos\theta\right), \tag{52a}$$

with

$$U = \frac{c}{\sqrt{2}}\sqrt{\mu\epsilon + \mu^2\alpha''^2 - \frac{\mu^2}{4\omega^2}b^2\cos^2\theta}, \tag{52b}$$

$$A_\pm = \sqrt{\sqrt{1+\left(\frac{\mu^2\alpha'' b\cos\theta}{\omega(\mu\epsilon+\mu^2\alpha''^2) - \frac{\mu^2 b^2}{4\omega}\cos^2\theta}\right)^2} \pm 1}. \tag{52c}$$

We point out that there is a frequency window at which U is purely imaginary, i.e., for $0 < \omega < \omega_0$, where ω_0 is

$$\omega_0 = \frac{1}{2}\sqrt{\frac{\mu b^2\cos^2\theta}{\epsilon + \mu\alpha''^2}}, \tag{53}$$

while $A_\pm$ remains real. In this range, the refractive indices are given by

$$n_\pm = \mp U'A_- \mp \mu c\alpha'' + i\left(U'A_+ - \frac{\mu c}{2\omega}b\cos\theta\right), \tag{54}$$

with

$$U' = \frac{c}{\sqrt{2}}\sqrt{\frac{\mu^2}{4\omega^2}b^2\cos^2\theta - \mu\epsilon - \mu^2\alpha''^2}. \tag{55}$$

Therefore, two main scenarios arise: (i) For $0 < \omega < \omega_0$, the refractive indices are given by Eq. (54), and (ii) for $\omega > \omega_0$, they are described by Eq. (52a). The physical consequences of this feature will be examined later, with a focus on the rotatory power.

Considering the circular polarization of the propagating modes (50), the rotatory power (35) represents properly the birefringence effects. Thus, for the refractive indices given in Eq. (52), one achieves

$$\delta = \mu\omega\alpha'', \tag{56}$$

defined for the regime $\omega > \omega_0$, where U is real. Differently from the previous scenario of Sec. III A, the rotatory power (56) cannot undergo a sign reversion. Furthermore, the result in Eq. (56) recovers the same result obtained in Ref. [28], so that the magnetic conductivity does not contribute in this frequency range.

On the other hand, for the frequency window $0 < \omega < \omega_0$, the refractive indices are the ones of Eq. (54), yielding the following rotatory:

$$\delta = \frac{\omega A_-}{\sqrt{2}}\sqrt{\frac{\mu^2}{4\omega^2}b^2\cos^2\theta - \mu\epsilon - \mu^2\alpha''^2} + \mu\omega\alpha''. \tag{57}$$

It is worth mentioning that $\delta > 0$ for $\alpha'' < 0$ or $\alpha'' > 0$ and that Eq. (57) holds only in the frequency range $0 < \omega < \omega_0$.

The behavior of the rotatory power for the entire frequency domain is obtained by plotting Eq. (57) at $0 < \omega < \omega_0$ and Eq. (56) at $\omega > \omega_0$, with a discontinuity at $\omega = \omega_0$, as illustrated in Fig. 2. In more detail, we highlight the following: (1) For $\alpha'' > 0$, the rotatory power is always positive, with a discontinuity at $\omega = \omega_0$, indicating clockwise rotation of a linear polarization wave, and (2) for $\alpha'' < 0$, the rotatory power is positive for $0 < \omega < \omega_0$, and negative for $\omega > \omega_0$, with discontinuity and sign reversal at the frequency $\omega = \omega_0$.

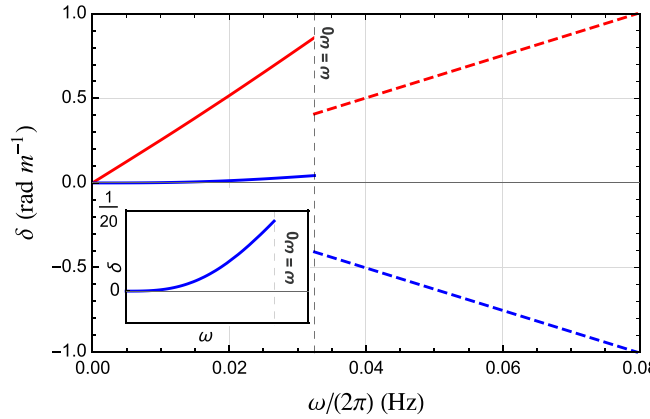

FIG. 2. Rotatory power of Eqs. (56) and (57). The solid lines indicate the rotatory power (57) defined in the region $0 < \omega < \omega_0$. The dashed curves represent the rotatory power (56) in the region $\omega > \omega_0$. The vertical dashed line is given by $\omega_0/(2\pi) = 1/(4\pi\sqrt{6})$ Hz, with ω_0 of Eq. (53). Here, we have used $\mu = 1\ \mathrm{H\,m^{-1}}$, $\epsilon = 2\ \mathrm{F\,m^{-1}}$, $b = 1\ \Omega^{-1}\,\mathrm{s^{-1}}$, $\cos^2\theta = 1$, and $\alpha'' = 2\ \mathrm{F\,s^{-1}}$ (red lines) and $\alpha'' = -2\ \mathrm{F\,s^{-1}}$ (blue curves). The inset plot highlights the behavior of δ (57) in the regime $0 < \omega < \omega_0$.

The RP (57) exhibits a sign reversal (when $\alpha'' < 0$) and also discontinuity at the frequency $\omega = \omega_0$. This happens because δ assumes different functional forms for the two frequency intervals under examination. Indeed, for $0 < \omega < \omega_0$, δ is defined by Eq. (57), while for $\omega > \omega_0$ it is given by Eq. (56).

Another relevant point is that the modes are absorbed to a different degree when $\omega > \omega_0$. This difference is characterized by the dichroism coefficient, defined as

$$\delta_d = -\frac{\omega}{2c}[\mathrm{Im}(n_+) - \mathrm{Im}(n_-)], \tag{58}$$

which for Eq. (52) yields

$$\delta_d = -\frac{\omega U}{c}\sqrt{\sqrt{1+\left(\frac{\mu^2c^2\alpha'' b\cos\theta}{2\omega U^2}\right)^2} - 1}. \tag{59}$$

The behavior of δ_d for $\cos\theta = \pm 1$ in terms of the frequency $\omega/(2\pi)$ is depicted in Fig. 3, which reveals the absence and presence of dichroism for $\omega < \omega_0$ and $\omega > \omega_0$, respectively. For $\omega > \omega_0$, the LCR mode, $\mathbf{E}_+$, is more absorbed than the RCP mode, $\mathbf{E}_-$, that is, $\delta_d < 0$. Furthermore, it does not occur δ_d sign reversal.

3. Optical effects for non-null Ohmic and magnetic conductivity, $\sigma_{ij}^B \neq 0$, $\sigma \neq 0$

Let us now address the bi-isotropic medium endowed with both magnetic conductivity σ_{ij}^B of Eq. (40) and Ohmic conductivity σ as considered in Eq. (46). Remembering that $\tilde{\epsilon} = \epsilon + i\sigma/\omega$, the refractive indices (40) are now cast at the form

$$n_\pm = U(A'_\pm \pm iA''_\pm) \mp \mu c\alpha'' - i\frac{\mu c}{2\omega}b\cos\theta, \tag{60}$$

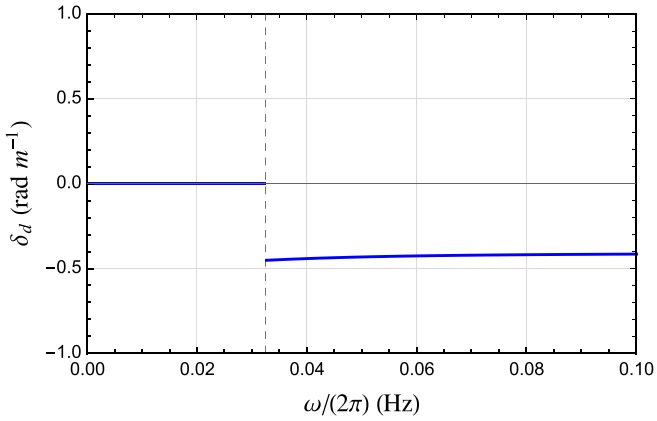

FIG. 3. Dichroism coefficient of Eq. (59) in terms of $\omega/(2\pi)$. Here, we have used $\mu = 1\ \mathrm{H\,m^{-1}}$, $\epsilon = 2\ \mathrm{F\,m^{-1}}$, $\alpha'' = 2\ \mathrm{F\,s^{-1}}$, $b = 1\ \Omega^{-1}\,\mathrm{s^{-1}}$, and $\cos\theta = \pm 1$.

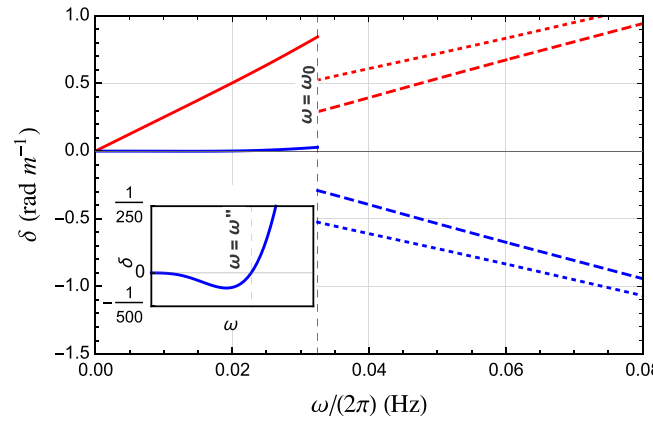

FIG. 4. Rotatory power of Eqs. (63) and (63). The solid lines indicate the rotatory power (65) defined in the region $0 < \omega < \omega_0$. The dashed curves represent the rotatory power (63) defined in the region $\omega > \omega_0$ for $\cos\theta = 1$, and the dotted red lines represent (63) for $\cos\theta = -1$. The vertical dashed line is given by $\omega_0/(2\pi) = 1/(4\pi\sqrt{6})$ Hz, with ω_0 of Eq. (53). Here, we have used $\mu = 1\ \mathrm{H\,m^{-1}}$, $\epsilon = 2\ \mathrm{F\,m^{-1}}$, $b = 1\ \Omega^{-1}\,\mathrm{s^{-1}}$, $\sigma = 1\ \Omega^{-1}\,\mathrm{m^{-1}}$, $\alpha'' = 2\ \mathrm{F\,s^{-1}}$ (red lines) and $\alpha'' = -2\ \mathrm{F\,s^{-1}}$ (blue curves). The inset plot highlights the behavior of δ (65) in the regime $0 < \omega < \omega_0$, in which the vertical dashed line indicates the frequency $\omega''/(2\pi) \approx 0.0184$ Hz, the root of (65) in this frequency regime.

with

$$A'_{\pm} = \sqrt{\sqrt{1 + \left(\frac{\mu^2\alpha'' b\cos\theta \pm \mu\sigma}{\omega(\mu\epsilon + \mu^2\alpha''^2) - \mu^2 b^2\cos^2\theta/4\omega}\right)^2} + 1}, \tag{61}$$

$$A''_{\pm} = \sqrt{\sqrt{1 + \left(\frac{\mu^2\alpha'' b\cos\theta \pm \mu\sigma}{\omega(\mu\epsilon + \mu^2\alpha''^2) - \mu^2 b^2\cos^2\theta/4\omega}\right)^2} - 1}. \tag{62}$$

For the frequency range $\omega > \omega_0$, U is real, so that the refractive indices are given as presented in Eq. (60), with which the rotatory power is

$$\delta = \mu\omega\alpha'' - \frac{\omega U}{2c}(A'_+ - A'_-). \tag{63}$$

For the frequency range $0 < \omega < \omega_0$, where U is purely imaginary, the refractive indices are

$$n_{\pm} = \mp U' A''_{\pm} \mp \mu c\alpha'' + i\left(U' A'_{\pm} - \frac{\mu c}{2\omega} b\cos\theta\right), \tag{64}$$

yielding the following rotatory power:

$$\delta = \mu\omega\alpha'' + \frac{\omega U'}{2c}(A''_+ + A''_-). \tag{65}$$

To better understand the effect of the Ohmic conductivity in this scenario, we illustrate in Fig. 4 the rotatory power for the entire frequency domain, obtained by plotting Eq. (65) for $0 < \omega < \omega_0$ and Eq. (63) for $\omega > \omega_0$.

Comparing Figs. 2 and 4, we remark on some aspects:

(1) In the region $\omega > \omega_0$, the rotatory power exhibits linear and slightly different behaviors for $\cos\theta = 1$ or $\cos\theta = -1$ (see the dotted and dashed lines, respectively). This is a consequence of the linear factor $\cos\theta$ that appears in the numerator of expressions (61) and (62) and the minus relative sign between A'_+ and A'_- in expression (63).

(2) For $0 < \omega < \omega_0$ and $\alpha'' > 0$, the rotatory power increases monotonically with ω, being quite similar to the one obtained for $\sigma = 0$ (see the red continuous line in Fig. 2).

(3) For $0 < \omega < \omega_0$ and $\alpha'' < 0$, the rotatory power possesses a small magnitude around zero and a nonlinear behavior. Starting from zero, it first slightly diminishes, reaching a negative minimum value. It then increases, becoming positive at a special frequency ω'', where δ changes sign. We thus observe that the RP undergoes sign reversal inside the range $0 < \omega < \omega_0$, a distinction in relation to the pattern of Fig. 2.

Concerning the results of Fig. 4 we still mention that the distinction observed in the propagation for $\cos\theta = 1$ and $\cos\theta = -1$ does not appear in the range $0 < \omega < \omega_0$. The reason is the relative plus sign in the sum $A''_+ + A''_-$ that composes the RP (65). Such a sign turns this term equal for $\theta = 0$ or $\theta = \pi$. The propagation difference observed in the region $\omega > \omega_0$ may work as a tool to distinguish between propagation parallel or antiparallel to the vector **b** and as a measure of the relative magnitude of Ohmic conductivity in relation to the magnetic conductivity.

Finally, it remains to examine the dichroism coefficient, which for the region $0 < \omega < \omega_0$ is given by

$$\delta_d = -\frac{\omega}{2c} U'(A'_+ - A'_-), \tag{66}$$

while for the range $\omega > \omega_0$ reads

$$\delta_d = -\frac{\omega}{2c} U(A''_+ + A''_-). \tag{67}$$

The behavior of the dichroism in the entire frequency domain is depicted in Fig. 5.

IV. FINAL REMARKS

In this paper, we have examined the classical electromagnetic propagation in bi-isotropic media supporting magnetic current associated with the CME, describing optical effects of the medium. For the full isotropic case of Sec. III A, defined

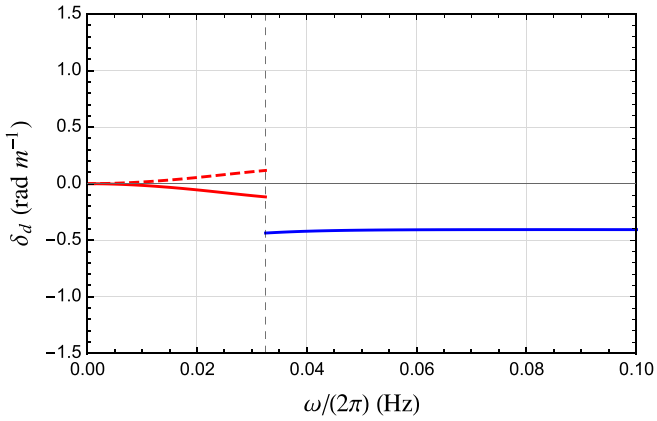

FIG. 5. Dichroism coefficient. The red lines indicate dichroism of Eq. (66) for $\cos\theta = 1$ (solid line) and $\cos\theta = -1$ (dashed curve). The blue line illustrates the behavior of Eq. (67) for $\cos\theta = \pm 1$. Here, we have used $\mu = 1\ \mathrm{H\,m^{-1}}$, $\epsilon = 2\ \mathrm{F\,m^{-1}}$, $\alpha'' = 2\ \mathrm{F\,s^{-1}}$, and $b = 1\ \Omega^{-1}\,\mathrm{s^{-1}}$.

by bi-isotropic constitutive relations and isotropic magnetic conductivity, we have found circularly polarized propagating modes, yielding circular birefringence expressed in terms of the linear dispersive RP (37). It experiences sign reversal at the frequency $\omega = \omega'$, with ω' given by Eq. (38). Such an effect only occurs when $\Sigma \neq 0$ and $\alpha'' < 0$.

In the scenario of Sec. III B, the bi-isotropic dielectric is endowed with Ohmic conductivity and an asymmetric magnetic current represented by the antisymmetric conductivity tensor parametrized in terms of the constant 3-vector **b**, as pointed out in Eq. (40). The propagating modes are composed of a transversal sector, described by circular polarizations, and a longitudinal component. For the **b**-longitudinal special case, the electric fields recover left- and right-handed circularly polarized vectors. The optical effects of this system were discussed for two scenarios: $\sigma^B_{ij} \neq 0$ and $\sigma = 0$ and $\sigma^B_{ij} \neq 0$ and $\sigma \neq 0$.

In Sec. III B 2, the bi-isotropic medium is considered only under the effect of the chiral conductivity (and $\sigma = 0$). The refractive indices were carried out and the birefringence was examined in terms of the RP considering two frequency intervals: (i) $0 < \omega < \omega_0$ and (ii) $\omega > \omega_0$, with ω_0 of Eq. (53). We have obtained an involved dispersive RP, which exhibits a discontinuity at $\omega = \omega_0$ and changes sign whenever $\alpha'' < 0$.

In Sec. III B 3, the bi-isotropic dielectric was considered under the presence of both Ohmic and chiral magnetic conductivities. The RP was evaluated, exhibiting discontinuity and reversion, the same main features observed in the case of Sec. III B 2, but with some additional particularities scrutinized in Fig. 4. Dicrohism was also examined, being endowed with discontinuity in both cases.

The RP reversal found here is not observed in usual dielectrics, being reported in rotating plasmas [49], graphene systems [51], and Weyl metals and semimetals with low electron density endowed with chiral conductivity [81]. Comparing the latter chiral Weyl metal with the scenario of Sec. III B 2, we observe some differences, however. In Ref. [81] the RP presents sign reversal without undergoing discontinuity. In the present bi-isotropic dielectric with magnetic conductivity, the RP undergoes reversal with discontinuity. Furthermore, we still notice some additional distinctions. While the RP magnitude of Eqs. (37) and (56) increases linearly with ω for high frequencies, the RP of a dielectric chiral medium [81] or Weyl semimetal [82] decreases with $1/\omega^2$ at this frequency domain. The unusual features here reported may provide a channel to characterize bi-isotropic media with chiral conductivity. Indeed, it may be used to distinguish the bi-isotropic scenario with antisymmetric chiral conductivity, described by constitutive relations (40), from the bi-isotropic medium endowed with isotropic magnetic conductivity (17).

When the rotatory power δ is positive (negative), the medium is defined as right (left) handed, since it rotates the plane of linear polarization light in the clockwise (counterclockwise) direction [33,34]. This definition characterizes the handedness of the medium considering the optical rotation of the linear polarization wave. Thus, the rotatory power inversion reported here also reveals a handedness reversal of the bi-isotropic dielectric (with $\alpha'' < 0$) under the presence of the magnetic current. Concerning the results of Sec. III A, as illustrated in Fig. 1 (blue line), for $\omega < \omega'$ the medium is right handed, while for $\omega > \omega'$ it becomes left handed. In the antisymmetric case of Sec. III B, Fig. 2 (blue line) shows a right-handed medium for $0 < \omega < \omega_0$, and a left-handed medium for $\omega > \omega_0$. This can open an interesting connection between electromagnetic chirality/helicity [35,83–86] and the combined constitutive relations examined in this paper.

ACKNOWLEDGMENTS

The authors express their gratitude to FAPEMA, CNPq, and CAPES (Brazilian research agencies) for their invaluable financial support. M.M.F. is supported by FAPEMA Universal/01187/18, CNPq/Produtividade 311220/2019-3 and CNPq/Universal/422527/2021-1. Furthermore, we are indebted to CAPES/Finance Code 001 and FAPEMA/POS-GRAD-02575/21.

[1] J. D. Jackson, *Classical Electrodynamics*, 3rd ed. (Wiley, New York, 1999).

[2] A. Zangwill, *Modern Electrodynamics* (Cambridge University Press, New York, 2012).

[3] I. V. Lindell, A. H. Sihvola, S. A. Tretyakov, and A. J. Viitanen, *Electromagnetic Waves in Chiral and Bi-Isotropic Media* (Artech House, Boston, 1993).

[4] J. A. Kong, *Electromagnetic Wave Theory* (Wiley, New York, 1986).

[5] J. F. Nieves and P. B. Pal, Third electromagnetic constant of an isotropic medium, Am. J. Phys. **62**, 207 (1994).

[6] R. C. Gauthier, Bi-anisotropic resonators analyzed using Fourier–Bessel numerical formulation; Sagnac effect application, Opt. Commun. **435**, 413 (2019).

[7] Y. T. Aladadi and M. A. S. Alkanhal, Classification and characterization of electromagnetic materials, Sci. Rep. **10**, 11406 (2020).

[8] A. H. Sihvola and I. V. Lindell, Bi-isotropic constitutive relations, Microw. Opt. Technol. Lett. **4**, 295 (1991).

[9] A. H. Sihvola and I. V. Lindell, Properties of bi-isotropic Fresnel reflection coefficients, Opt. Commun. **89**, 1 (1992).

[10] M.-C. Chang and M.-F. Yang, Optical signature of topological insulators, Phys. Rev. B **80**, 113304 (2009).

[11] A. Martín-Ruiz, M. Cambiaso, and L. F. Urrutia, The magnetoelectric coupling in electrodynamics, Int. J. Mod. Phys. A **34**, 1941002 (2019).

[12] A. Martín-Ruiz, M. Cambiaso, and L. F. Urrutia, Electro- and magnetostatics of topological insulators as modeled by planar, spherical, and cylindrical θ boundaries: Green's function approach, Phys. Rev. D **93**, 045022 (2016).

[13] A. Lakhtakia and T. G. Mackay, Classical electromagnetic model of surface states in topological insulators, J. Nanophotonics **10**, 033004 (2016).

[14] T. M. Melo, D. R. Viana, W. A. Moura-Melo, J. M. Fonseca, and A. R. Pereira, Topological cutoff frequency in a slab waveguide: Penetration length in topological insulator walls, Phys. Lett. A **380**, 973 (2016).

[15] Z.-X. Li, Y. Cao, and P. Yan, Topological insulators and semimetals in classical magnetic systems, Phys. Rep. **915**, 1 (2021).

[16] R. Li, J. Wang, X.-L. Qi, and S.-C. Zhang, Dynamical axion field in topological magnetic insulators, Nat. Phys. **6**, 284 (2010).

[17] A. Sekine and K. Nomura, Axion electrodynamics in topological materials, J. Appl. Phys. **129**, 141101 (2021).

[18] M. E. Tobar, B. T. McAllister, and M. Goryachev, Modified axion electrodynamics as impressed electromagnetic sources through oscillating background polarization and magnetization, Phys. Dark Universe **26**, 100339 (2019).

[19] L. H. C. Borges, A. G. Dias, A. F. Ferrari, J. R. Nascimento, and A. Yu. Petrov, Generation of axionlike couplings via quantum corrections in a Lorentz-violating background, Phys. Rev. D **89**, 045005 (2014).

[20] V. A. De Lorenci and G. P. Goulart, Magnetoelectric birefringence revisited, Phys. Rev. D **78**, 045015 (2008).

[21] J. M. A. Paixão, L. P. R. Ospedal, M. J. Neves, and J. A. Helayël-Neto, The axion-photon mixing in non-linear electrodynamic scenarios, arXiv:2205.05442.

[22] P. Gaete and J. A. Helayel-Neto, Vacuum material properties and Cherenkov radiation in logarithmic electrodynamics, arXiv:2205.03252.

[23] P. Gaete and J. A. Helayël-Neto, Remarks on inverse electrodynamics, Eur. Phys. J. C **81**, 899 (2021); A note on nonlinear electrodynamics, Europhys. Lett. **119**, 51001 (2017); P. Gaete, J. A. Helayël-Neto, and L. P. R. Ospedal, Coulomb's law modification driven by a logarithmic electrodynamics, *ibid.* **125**, 51001 (2019).

[24] Y. Itin, Dispersion relation for electromagnetic waves in anisotropic media, Phys. Lett. A **374**, 1113 (2010).

[25] N. J. Damaskos, A. L. Maffett, and P. L. E. Uslenghi, Dispersion relation for general anisotropic media, IEEE Trans. Antennas Propagat. **30**, 991 (1982).

[26] S.-R. Lin, R.-Y. Zhang, Y.-R. Ma, W. Jia, and Q. Zhaoa, Electromagnetic wave propagation in time-dependent media with antisymmetric magnetoelectric coupling, Phys. Lett. A **380**, 2582 (2016).

[27] S. Ougier, I. Chenerie, A. Sihvola, and A. Priou, Propagation in bi-isotropic media: Effect of different formalisms on the propagation analysis, Prog. Electromagn. Res. **09**, 19 (1994).

[28] P. D. S. Silva, R. Casana, and M. M. Ferreira, Jr., Symmetric and antisymmetric constitutive tensors for bi-isotropic and bi-anisotropic media, Phys. Rev. A **106**, 042205 (2022).

[29] J. Mun *et al.*, Electromagnetic chirality: From fundamentals to nontraditional chiroptical phenomena, Light: Sci. Appl. **9**, 139 (2020).

[30] P. Hillion, Manifestly covariant formalism for electromagnetism in chiral media, Phys. Rev. E **47**, 1365 (1993).

[31] S. Kaushik, Magnetic and optical response of chiral fermions, arXiv:2112.13749.

[32] L. D. Barron, *Molecular Light Scattering and Optical Activity*, 2nd ed. (Cambridge University Press, New York, 2004).

[33] E. Hecht, *Optics*, 4nd ed. (Addison Wesley, San Francisco, 2002).

[34] G. H. Wagniere, *On Chirality and the Universal Asymmetry: Reflections on Image and Mirror Image* (Wiley-VCH, Weinheim, 2007).

[35] Y. Tang and A. E. Cohen, Optical Chirality and Its Interaction with Matter, Phys. Rev. Lett. **104**, 163901 (2010).

[36] G. R. Fowles, *Introduction to Modern Optics*, 2nd ed. (Dover., New York, 1975); A. K. Bain, *Crystal Optics: Properties and Applications* (Wiley-VCH, Weinheim, 2019).

[37] E. U. Condon, Theories of Optical Rotatory Power, Rev. Mod. Phys. **9**, 432 (1937).

[38] H. S. Bennett and E. A. Stern, Faraday effect in solids, Phys. Rev. **137**, A448 (1965); L. M. Roth, Theory of the Faraday effect in solids Faraday effect in solids, *ibid.* **133**, A542 (1964).

[39] L. Ohnoutek, M. Hakl, M. Veis, B. A. Piot, C. Faugeras, G. Martinez, M. V. Yakushev, R. W. Martin, Č. Drašar, A. Materna, G. Strzelecka, A. Hruban, M. Potemski, and M. Orlita, Strong interband Faraday rotation in 3D topological insulator Bi_2Se_3, Sci. Rep. **6**, 19087 (2016).

[40] W.-K. Tse and A. H. MacDonald, Giant Magneto-Optical Kerr Effect and Universal Faraday Effect in Thin-Film Topological Insulators, Phys. Rev. Lett. **105**, 057401 (2010); Magneto-optical and magnetoelectric effects of topological insulators in quantizing magnetic fields, Phys. Rev. B **82**, 161104(R) (2010); Magneto-optical Faraday and Kerr effects in topological insulator films and in other layered quantized Hall systems, **84**, 205327 (2011).

[41] J. Maciejko, X.-L. Qi, H. D. Drew, and S.-C. Zhang, Topological Quantization in Units of the Fine Structure Constant, Phys. Rev. Lett. **105**, 166803 (2010).

[42] I. Crassee, J. Levallois, A. L. Walter, M. Ostler, A. Bostwick, E. Rotenberg, T. Seyller, D. van der Marel, and A. B. Kuzmenko, Giant Faraday rotation in single- and multilayer graphene, Nat. Phys. **7**, 48 (2011).

[43] R. Shimano, G. Yumoto, J. Y. Yoo, R. Matsunaga, S. Tanabe, H. Hibino, T. Morimoto, and H. Aoki, Quantum Faraday and Kerr rotations in graphene, Nat. Commun. **4**, 1841 (2013).

[44] L. Tschugaeff, Anomalous rotatory dispersion, Trans. Faraday Soc. **10**, 70 (1914).

[45] R. E. Newnham, *Properties of Materials - Anisotropy, Symmetry, Structure* (Oxford University Press, New York, 2005).

[46] D. G. Dimitriu and D. O. Dorohoi, New method to determine the optical rotatory dispersion of inorganic crystals applied to some samples of Carpathian Quartz, Spectrochim. Acta, Part A **131**, 674 (2014).

[47] L. A. Pajdzik and A. M. Glazer, Three-dimensional birefringence imaging with a microscope tilting-stage. I. Uniaxial crystals, J. Appl. Crystallogr. **39**, 326 (2006).

[48] X. Liu, J. Yang, Z. Geng, and H. Jia, Simultaneous measurement of optical rotation dispersion and absorption spectra for chiral substances, Chirality **32**, 1072 (2022).

[49] R. Gueroult, J.-M. Rax, and N. J. Fisch, Enhanced tuneable rotatory power in a rotating plasma, Phys. Rev. E **102**, 051202(R) (2020).

[50] R. Gueroult, Y. Shi, J.-M. Rax, and N. J. Fisch, Determining the rotation direction in pulsars, Nat. Commun. **10**, 3232 (2019).

[51] J.-M. Poumirol, P. Q. Liu, T. M. Slipchenko, A. Y. Nikitin, L. Martin-Morento, J. Faist, and A. B. Kuzmenko, Electrically controlled terahertz magneto-optical phenomena in continuous and patterned graphene, Nat. Commun. **8**, 14626 (2017).

[52] I. Tutunnikov, U. Steinitz, E. Gershnabel, J-M. Hartmann, A. A. Milner, V. Milner, and I. Sh. Averbukh, Rotation of the polarization of light as a tool for investigating the collisional transfer of angular momentum from rotating molecules to macroscopic gas flows, Phys. Rev. Res. **4**, 013212 (2022).

[53] U. Steinitz and I. Sh. Averbukh, Giant polarization drag in a gas of molecular super-rotors, Phys. Rev. A **101**, 021404(R) (2020).

[54] N. Tischler, M. Krenn, R. Fickler, X. Vidal, A. Zeilinger, and G. Molina-Terriza, Quantum optical rotatory dispersion, Sci. Adv. **2**, e1601306 (2016).

[55] J. H. Woo, B. K. M. Gwon, J. H. Lee, D-W. Kim, W. Jo, D. H. Kim, and J. W. Wu, Time-resolved pump-probe measurement of optical rotatory dispersion in chiral metamaterial, Adv. Opt. Mater. **5**, 1700141 (2017).

[56] Q. Zhang, E. Plum, J.-Y. Ou, H. Pi, J. Li, K. F. MacDonald, and N. I. Zheludev, Electrogyration in metamaterials: Chirality and polarization rotatory power that depend on applied electric field, Adv. Optical Mater. **9**, 2001826 (2021).

[57] P. Hosur and X.-L. Qi, Tunable circular dichroism due to the chiral anomaly in Weyl semimetals, Phys. Rev. B **91**, 081106(R) (2015).

[58] M. Nieto-Vesperinas, Optical theorem for the conservation of electromagnetic helicity: Significance for molecular energy transfer and enantiomeric discrimination by circular dichroism, Phys. Rev. A **92**, 023813 (2015).

[59] Y. Tang and A. E. Cohen, Enhanced Enantioselectivity in Excitation of Chiral Molecules by Superchiral Light, Science **332**, 333 (2011).

[60] M. Amin, O. Siddiqui, and M. Farhat, Linear and Circular Dichroism in Graphene-Based Reflectors for Polarization Control, Phys. Rev. Appl. **13**, 024046 (2020).

[61] D. E. Kharzeev, The chiral magnetic effect and anomaly-induced transport, Prog. Part. Nucl. Phys. **75**, 133 (2014); D. E. Kharzeev, J. Liao, S. A. Voloshin, and G. Wang, Chiral magnetic and vortical effects in high-energy nuclear collisions–A status report, *ibid.* **88**, 1 (2016).

[62] D. Kharzeev, K. Landsteiner, A. Schmitt, and H. U. Yee, *Strongly Interacting Matter in Magnetic Fields*, Lecture Notes in Physics Vol. 871 (Springer, Berlin, 2013).

[63] K. Fukushima, D. E. Kharzeev, and H. J. Warringa, Chiral magnetic effect, Phys. Rev. D **78**, 074033 (2008).

[64] G. Inghirami, M. Mace, Y. Hirono, L. Del Zanna, D. E. Kharzeev, and M. Bleicher, Magnetic fields in heavy ion collisions: flow and charge transport, Eur. Phys. J. C **80**, 293 (2020).

[65] A. F. Bubnov, N. V. Gubina, and V. Ch. Zhukovsky, Vacuum current induced by an axial-vector condensate and electron anomalous magnetic moment in a magnetic field, Phys. Rev. D **96**, 016011 (2017).

[66] A. A. Burkov, Chiral anomaly and transport in Weyl metals, J. Phys.: Condens. Matter **27**, 113201 (2015).

[67] M.-C. Chang and M.-F. Yang, Chiral magnetic effect in a two-band lattice model of Weyl semimetal, Phys. Rev. B **91**, 115203 (2015).

[68] E. C. I. van der Wurff and H. T. C. Stoof, Anisotropic chiral magnetic effect from tilted Weyl cones, Phys. Rev. B **96**, 121116(R) (2017).

[69] K. Landsteiner, Anomalous transport of Weyl fermions in Weyl semimetals, Phys. Rev. B **89**, 075124 (2014).

[70] S. Kaushik and D. E. Kharzeev, Quantum oscillations in the chiral magnetic conductivity, Phys. Rev. B **95**, 235136 (2017).

[71] A. Martín-Ruiz, M. Cambiaso, and L. F. Urrutia, Electromagnetic fields induced by an electric charge near a Weyl semimetal, Phys. Rev. B **99**, 155142 (2019).

[72] K. Deng, J. S. Van Dyke, D. Minic, J. J. Heremans, and E. Barnes, Exploring self-consistency of the equations of axion electrodynamics in Weyl semimetals, Phys. Rev. B **104**, 075202 (2021).

[73] R. E. Throckmorton, J. Hofmann, E. Barnes, and S. D. Sarma, Many-body effects and ultraviolet renormalization in three-dimensional Dirac materials, Phys. Rev. B **92**, 115101 (2015).

[74] E. Barnes, J. J. Heremans, and D. Minic, Electromagnetic Signatures of the Chiral Anomaly in Weyl Semimetals, Phys. Rev. Lett. **117**, 217204 (2016).

[75] F. Wilczek, Two Applications of Axion Electrodynamics, Phys. Rev. Lett. **58**, 1799 (1987).

[76] Z. Qiu, G. Cao, and X.-G. Huang, Electrodynamics of chiral matter, Phys. Rev. D **95**, 036002 (2017).

[77] P. D. S. Silva, M. M. Ferreira, Jr. M. Schreck, and L. F. Urrutia, Magnetic-conductivity effects on electromagnetic propagation in dispersive matter, Phys. Rev. D **102**, 076001 (2020).

[78] S. Kaushik, D. E. Kharzeev, and E. J. Philip, Transverse chiral magnetic photocurrent induced by linearly polarized light in symmetric Weyl semimetals, Phys. Rev. Res. **2**, 042011(R) (2020).

[79] P. D. S. Silva, L. Lisboa-Santos, M. M. Ferreira, Jr. and M. Schreck, Effects of CPT-odd terms of dimensions three and five on electromagnetic propagation in continuous matter, Phys. Rev. D **104**, 116023 (2021).

[80] A. Kostelecky, R. Lehnert, N. McGinnis, M. Schreck, and B. Seradjeh, Lorentz violation in Dirac and Weyl semimetals, Phys. Rev. Res. **4**, 023106 (2022).

[81] J. Ma and D. A. Pesin, Dynamic Chiral Magnetic Effect and Faraday Rotation in Macroscopically Disordered Helical Metals, Phys. Rev. Lett. **118**, 107401 (2017).

[82] U. Dey, S. Nandy, and A. Taraphder, Dynamic chiral magnetic effect and anisotropic natural optical activity of tilted Weyl semimetals, Sci. Rep. **10**, 2699 (2020).

[83] R. P. Cameron, S. M. Barnett, and A. M. Yao, Optical helicity, optical spin and related quantities in electromagnetic theory, New J. Phys. **14**, 053050 (2012).

[84] K. Y. Bliokh and F. Nori, Dual electromagnetism: Helicity, spin, momentum and angular momentum, New J. Phys. **15**, 033026 (2013); K. Y. Bliokh, A. Y. Bekshaev, and F. Nori, Corrigendum: Dual electromagnetism: Helicity, spin, momentum, and angular momentum, *ibid.* **18**, 089503 (2016); Conservation of the spin and orbital angular momenta in electromagnetism, **16**, 093037 (2014).

[85] M. F. Guasti, Chirality, helicity and the rotational content of electromagnetic fields, Phys. Lett. A **383**, 3180 (2019).

[86] C.-W. Qiu, H.-Y. Yao, L.-W. Li, S. Zouhdi, and T.-S. Yeo, Routes to left-handed materials by magnetoelectric couplings, Phys. Rev. B **75**, 245214 (2007).